MOLECULAR AND CELLULAR BIOLOGY, Nov. 2007, p. 7538–7550 Vol. 27, No. 21
0270-7306/07/$08.00+0 doi:10.1128/MCB.00955-07

Activation of the RalGEF/Ral Pathway Promotes Prostate Cancer Metastasis to Bone▽‡

JuanJuan Yin,† Claire Pollock,† Kirsten Tracy, Monika Chock, Philip Martin, Michael Oberst, and Kathleen Kelly*

Cell and Cancer Biology Branch, Center for Cancer Research, National Cancer Institute, 37 Convent Drive, Room 1068, Bethesda, Maryland 20892

Received 30 May 2007/Returned for modification 19 July 2007/Accepted 13 August 2007

A hallmark of metastasis is organ specificity; however, little is known about the underlying signaling pathways responsible for the colonization and growth of tumor cells in target organs. Since tyrosine kinase receptor activation is frequently associated with prostate cancer progression, we have investigated the role of a common signaling intermediary, activated Ras, in prostate cancer metastasis. Three effector pathways downstream of Ras, Raf/extracellular signal-regulated kinase (ERK), phosphatidylinositol 3-kinase, and Ral guanine nucleotide exchange factors (RalGEFs), were assayed for their ability to promote the metastasis of a tumorigenic, nonmetastatic human prostate cancer cell line, DU145. Oncogenic Ras promoted the metastasis of DU145 to multiple organs, including bone and brain. Activation of the Raf/ERK pathway stimulated metastatic colonization of the brain, while activation of the RalGEF pathway led to bone metastases, the most common organ site for prostate cancer metastasis. In addition, loss of RalA in the metastatic PC3 cell line inhibited bone metastasis but did not affect subcutaneous tumor growth. Loss of Ral appeared to suppress expansive growth of prostate cancer cells in bone, whereas homing and initial colonization were less affected. These data extend our understanding of the functional roles of the Ral pathway and begin to identify signaling pathways relevant for organ-specific metastasis.

Cancer metastasis is the major determinant of cancer-related death. Metastasis is an inefficient process involving multiple steps that include local tumor cell dissemination, survival in the circulation, arrest in the vasculature, extravasation, and growth in distant organs (5). A hallmark of metastasis is the propensity of many types of cancers to metastasize to specific organs. Most circulating tumor cells passively arrest in capillary beds based upon mechanical constraints, and the organ selectivity for secondary growth of some cancers, such as colon cancer metastasis to liver, correlates with blood flow patterns (28, 41). However, it is clear from other examples, such as the predominant growth of breast and prostate cancer lesions in bone, an organ with relatively low arterial blood flow, that organ-specific factors other than hemodynamics determine metastatic colonization (24, 42).

It has been widely accepted that the final outcome of metastasis depends upon multiple interactions between metastatic cells and their host organ microenvironment (10). One type of specific interaction occurs as a result of vascular specialization in individual organs that may lead to the adherence of tumor cells to endothelial cells or other vascular elements (34). In addition, it is well established that after extravasation from the vessels, reciprocal interaction between tumor cells and stromal, parenchymal, and immune cells influences the likelihood of clonal growth (5).

The molecular mechanisms that determine metastatic competence and secondary organ specificity are poorly defined. Experimental and clinical studies have demonstrated that metastasis is an inefficient process whereby circulating tumor cells rarely colonize distant sites, leading to the hypothesis that successful metastatic cells carry a unique constellation of genetic changes in addition to those that give rise to the primary tumor (11). Consistent with this, recent investigations using the MDA-MB-231 breast cancer model have demonstrated that enhanced metastatic capacity can be selected from a heterogeneous tumor cell population and that organ-specific growth is closely linked with the expression of genes that encode factors such as secreted proteins and cell surface receptors that are necessary for interaction with the organ microenvironment (16, 20, 21). On the other hand, microarray analyses of several different types of primary adenocarcinomas have revealed a "poor prognosis" gene signature that is associated with metastasis and a negative clinical outcome (31, 38). Because the gene signature is contributed to by a large fraction of primary tumor cells, one interpretation of these data is that the signature reflects a predisposition to metastasis as opposed to the developed metastatic phenotype (3). Determining the signaling pathways that mediate metastasis and regulate genes that promote tissue-specific interactions is an important step in designing therapeutic strategies to treat and prevent metastasis.

Prostate cancer shows strong organ-specific metastasis to bone, and numerous pieces of evidence support the concept that tumor colonization of the bone is an active process involving reciprocal stimulation between prostate tumor cells and cellular elements in the bone matrix (19, 25). Prostate cancer is

* Corresponding author. Mailing address: Cell and Cancer Biology Branch, Center for Cancer Research, National Cancer Institute, 37 Convent Dr., Rm. 1068, Bethesda, MD 20892. Phone: (301) 435-4651. Fax: (301) 435-4655. E-mail: kellyka@mail.nih.gov.

† J.Y. and C.P. contributed equally to this study.

‡ Supplemental material for this article may be found at http://mcb.asm.org/.

▽ Published ahead of print on 20 August 2007.

androgen dependent such that initial androgen ablation therapy is effective in causing its regression. However, in most advanced prostate cancer, such treatment ultimately results in the recurrence of highly aggressive androgen-independent metastasis, most frequently in the bone (9). Increases in autocrine and paracrine growth factor loops are among the most commonly reported events that correlate with prostate cancer progression and are one mechanism of synergy with or replacement of androgen-dependent growth (2, 35). Many such growth factors and their cognate receptors, including epidermal growth factor, transforming growth factor α (TGF-α), keratinocyte growth factor, basic fibroblast growth factor, and insulin-like growth factor, signal through Ras-dependent pathways. Therefore, although Ras mutations in prostate cancer are rare, it is reasonable to propose that chronic Ras activation is a common feature of advanced metastatic prostate cancer (40).

Ras engages multiple downstream signaling pathways, including Raf protein kinase, phosphatidylinositol 3-kinase (PI3K), and members of the Ral guanine nucleotide exchange factor (RalGEF) family (32). While the Raf and PI3K pathways are well-validated effectors in cancers, investigations using human cancer cell lines and a mouse genetic model recently have shown that the RalGEF pathway also contributes to tumorigenesis and metastasis (8). Genetic ablation of RalGDS, a member of the Ras-activated RalGEF family, reduced the incidence and progression of tumors in a Ras-dependent mouse model of skin carcinogenesis (13).

An understanding of the cellular processes and the molecular mechanisms that mediate the biological responses to RalGEF/Ral activation is just beginning to emerge. RalGTP binds several effectors, resulting in the activation and/or coordination of various biological responses, including vesicle sorting, migration, and signal transduction (8). Effectors described to date include the Rac/Cdc42 GAP domain containing protein RalBP1 (4), the exocyst components Sec5 and Exo84 (23), filamin (27), and the Y box transcription factor, ZONAB (12). Binding of RalA-GTP to Sec5/Exo84 is directly implicated in regulating basolateral vesicle delivery, whereas Ral/RalBP1 has been indirectly implicated in endocytosis (8, 23). It seems likely that exocytotic and endocytotic processes will affect autocrine and paracrine signaling networks, both of which are expected to contribute to metastatic colonization.

RalGEFs activate RalA and RalB, two highly homologous GTPases. Although RalA and RalB have identical effector domains, the two proteins are differentially localized in cells and may have different affinities for effector proteins (8, 17, 36). In fact, distinct biological functions have been ascribed to RalA and RalB. For cell lines that express mutated oncogenic forms of Ras, such as human pancreatic cancer cell lines and genetically defined transformed human epithelial cell lines, RalA is almost always required for anchorage-independent growth in vitro and subcutaneous tumor growth in immunodeficient mice, whereas RalB is dispensable (17, 18). A small number of cancer cell lines of variable tissue origin with no obvious Ras mutations have been assayed for Ral-dependent growth properties (6). Transient RalA knockdown inhibited proliferation of suspended epithelial cells, and permanent RalA knockdown in a different study inhibited anchorage-independent growth in some of the cell lines assayed. Transient RalB knockdown in the presence but not the absence of RalA initiated programmed cell death in the three evaluated cancer cell lines. Thus, even in the absence of Ras mutations, RalA and RalB appear to play a role in the growth properties of several cancer cell lines (6). In addition to growth regulation, RalA and RalB contribute to migration and invasion. RalA and/or RalB have been found to be required for migration in various cell lines, although this is not always the case. With respect to migration, the interaction of the two pathways, as well as their redundancy, appears to be cell line dependent in the limited examples that have been investigated (18, 29).

In the present study, we investigated the effect of Ras-dependent signaling pathways upon the development of metastasis using two experimental xenograft models of prostate cancer. Activation of RalGEF was necessary and sufficient to promote the efficient growth of nonmetastatic DU145 cells specifically in bone, whereas other Ras-dependent pathways promoted brain metastasis. Consistent with a role for Ral in bone metastasis, knockdown of RalA inhibited the expansion of metastatic PC3 cells in the bone after initial colonization. These data begin to dissect underlying signaling pathways that preferentially support metastasis in distinct organs and emphasize the specificity of interactions between tumor cells and the organ microenvironment.

MATERIALS AND METHODS

Constructs. Mutant versions of the transforming human H-Ras^{V12} (Ras^{V12}) and its effector mutants Ras^{V12S35}, Ras^{V12G37}, Ras^{V12C40}, and RlfCAAX were subcloned into the pLC7ΔSX retroviral vector that directs the expression of CD7, allowing flow sorting of pLC7ΔSX-infected/CD7-positive cell lines (39). RalB^{N28} was cloned into pBABEpuro.

Lentiviral shRNA constitutive expression vectors against RalA and RalB were purchased from Open Biosystems in collaboration with the Broad Institute of Massachusetts Institute of Technology and Harvard RNAi consortium. RalA1 shRNA (5′-CCGGCGCTGCAATTAGAGACAACTACTCGAGTAGTTGTCTCTAATTGCAGCGTTTTT-3′), RalA2 shRNA (5′-CCGGCGAGCTAATGTTGACAAGGTACTCGAGTACCTTGTCAACATTAGCTCGTTTTT-3′), RalB1 shRNA (5′-CCGGCCTTTACAGCAACTGCCGAATCTCGAGATTCGGCAGTTGCTGTAAAGGTTTTTG-3′), and RalB2 shRNA (5′-CCGGCAAGGTGTTCTTTGACCTAATCTCGAGATTAGGTCAAAGAACACCTTGTTTTTG-3′) were supplied in a lentiviral expression vector, PLKO, which carries a puromycin selection marker. The vector, SFGnesTGL expressing a thymidine kinase/green fluorescent protein (GFP)/luciferase (TGL) fusion protein, was kindly provided by Gelovani Tjuvajev.

Cell culture and establishment of stable cell lines. DU145 and PC3 cells were obtained from the American Type Culture Collection (Manassas, VA) and cultured in RPMI 1640. HEK293FT and Amphophoenix cells were cultivated in Dulbecco modified Eagle medium. All media were supplemented with 10% fetal calf serum, 0.1 mM minimal essential medium nonessential amino acids, 2 mM L-glutamine, and 100 μg of gentamicin/ml. HEK293FT culture media also contained 500 μg of G418.

Establishment of cell lines stably expressing Ras effector domain mutant. DU145 stably expressing H-Ras^{V12}, one of three Ras effector domain mutants (H-Ras^{V12S35}, H-Ras^{V12G37}, and H-Ras^{V12C40}), or RlfCAAX were established by retroviral infection using standard protocols. One week after pLC7ΔSX infection, cells were harvested and labeled with anti-CD7-fluorescein isothiocyanate antibody (Pharmingen), and fluorescent cells were sorted two times until cells were >99% CD7 positive. A DU145Ras^{V12G37} cell line stably expressing pBABEpuro/RalB^{N28} was established by retroviral infection and selection with puromycin. DU145Ras^{V12G37} expressing the pBABEpuro vector (DU145Ras^{V12G37}puro) was used as a control.

Generation of luciferase-expressing lines. For bioluminescence imaging (BLI), parental DU145 and PC3 cells were infected with pSFGnesTGL (30), a retroviral vector that encodes a TGL fusion protein. Positive cells were isolated by fluorescence-activated cell sorting of GFP-expressing cells and subsequently infected with LC7ΔSX retroviruses containing oncogenic Ras^{V12} or its effector domain mutants. Positive cells were then sorted using both anti-CD7-PE and GFP fluorescence.

Generation of stable shRNA-expressing lines. DNAs (2.0 μg of VSV-G, 6.0 μg of psPAXII, and 8.0 μg of PLKO siRNA) were transfected into HEK293FT cells. Viral supernatants were harvested for infection of PC3 and DU145 cells. Positive cells were selected with puromycin (1.5 μg/ml).

Animal experiments. Six- to eight-week-old male athymic nude mice (Ncr *nu*/*nu*) were obtained from the National Cancer Institute, Frederick, MD. Animal care was provided in accordance with the procedures outlined in the *Guide for the Care and Use of Laboratory Animals.* Prior to inoculation, cells were treated with trypsin, resuspended in RPMI 1640–10% fetal calf serum, rotated at room temperature for 1 h, spun down, and washed in phosphate-buffered saline (PBS). Cells were counted and diluted to the appropriate concentration.

Tumorigenesis assays. A total of 5×10^6 PC3 cells in 50 μl was mixed 1:1 with growth factor-reduced Matrigel (Becton Dickinson) immediately prior to injection. DU145 cells were diluted to 2.5×10^6 in 0.1 ml of PBS. Cells were injected bilaterally subcutaneously into the flanks of nude mice. The tumor size was measured with calipers. The tumor volume was calculated from the following formula: tumor volume = $4/3\ \pi XL/2\ (W/2)^2$. The results represent mean ± the standard error (SE) for each experimental group.

Tumorigenesis in bone. Mice were anesthetized, the knees were flexed to a 90° angle, and a 27-gauge needle was inserted through the tibial plateau. A Hamilton syringe was used to accurately inject 25 μl of cells (10^5) into the proximal tibia. BLI and radiography were determined weekly to monitor the growth of tumor in bone. Mice were euthanized when they showed signs of morbidity or when bone lesions were obvious upon X-ray examination.

Systemic tumor metastasis. A total of 10^5 tumor cells in 0.1 ml of PBS were inoculated into the left cardiac ventricles of male nude mice after anesthetizing them with Avertin (500 mg/kg). To monitor the development of bone metastasis, the mice were radiographed weekly using an MX-20 Faxitron X-ray system (Faxitron). Mice were euthanized after weight loss of >10% body weight or after demonstrating signs of paralysis. Four long bones (two front limbs with scapulae and two hind limbs), spines, and soft tissues including the adrenal glands, kidney, spleen, liver, and brain were collected and fixed in 10% buffered formalin for histological analysis (HistoServ, Inc.). Necropsies were performed, and mice with evidence of tumor in the chest cavity were excluded from the study since this indicated excessive leakage of tumor cells during cardiac injection. Fewer than 5% of mice were excluded.

BLI and analysis. Mice were anesthetized with 1.5% isoflurane. D-Luciferin (Xenogen) was injected at 150 mg/kg (body weight). Five minutes later, bioluminescent images were acquired with an IVIS imaging system (Xenogen). Analysis was performed by using LivingImage software (Xenogen) by measuring the photon flux within a region of interest drawn around the bioluminescence signals. Blank regions of interest were also measured for each scan and deducted from each tumor photon flux to normalize. Ventral scans were used for quantification of all jaw and leg tumors. Dorsal scans were used for brain tumor quantifications.

Histology and histomorphometry. Long bones and spine were decalcified in 10% EDTA and embedded in paraffin. Sections were stained with hematoxylin, eosin, orange G, and phloxin (hematoxylin and eosin, orange G). Images of tissues and bones were acquired, and the total tumor area in each of four limbs was measured using the MetaMorph imaging system. All soft tissues were stained with hematoxylin and eosin. Human cytokeratin 18 was used as a marker to detect tumors or micrometastases in brain and soft tissues. Slides were autoclaved at 121°C for 10 min in sodium citrate buffer (10 mM sodium citrate, 0.05% Tween 20 [pH 6.0]) to retrieve antigen, followed by immunohistochemical staining with a mouse anti-human CK18 monoclonal antibody (Dako).

In vitro growth determinations. Cells were seeded in six replicates in 96-well plates at densities of 2×10^3 and 5×10^3 cells per well for DU145 and PC3, respectively. Each day, one plate was stained with crystal violet fixative solution for 30 min, rinsed in distilled water, and allowed to air dry. At the end of the experiment, crystal violet was dissolved by adding 100 μl of 50% ethanol containing 0.1 M sodium citrate to each well, and the absorbance was quantified at a 540-nm wavelength on a plate reader.

In vitro luciferase assays. Cells were seeded in triplicate in 24-well plates at a density of 10^5 cells per well. The following day the cells in two wells were lysed in 100 μl of Bright-Glo luciferase assay buffer (Promega). The cells were gently scraped by using a pipette tip, lysates were transferred to a 5-ml polystyrene round-bottom tube, and the light output measured by using a luminometer. The cells in the third well were treated with trypsin and counted by using a hemacytometer. Relative light unit readings were divided by cell number to obtain RLU/cell.

Distribution of fluorescent cells within organ vasculature. DU145 cells expressing empty vector (EV), Ras^{V12}, or Ras effector mutants were labeled with SNARF-1 carboxylic acid acetate succinimidyl ester (Molecular Probes) before inoculation. Mice were sacrificed 5 h after intracardiac injection; the bone, brain, and other soft tissues, including the kidneys and adrenal glands, were removed and kept on ice. Fluorescent cells in various organs were counted under a fluorescence stereomicroscope (Leica MZFLIII; excitation filter, 545/30 nm; barrier filter, 620/60 nm) with a ×1.6 planapochromatic objective lens at zoom position 8. Refocusing was performed when necessary to follow the contour of the tissues. Representative sections from soft tissues, including the brain (four sections), kidneys (two sections), and adrenal glands (one section), were counted for fluorescent cells. Four long bones (two tibia and two femurs) were counted for each mouse. To count cells from the bones, muscles were carefully removed from tibias and femurs without disturbing the blood vessels on the bone surfaces. Images were then captured by using a QImaging micropublisher charge-coupled device camera.

PTHrP assay. Parathyroid hormone-related protein (PTHrP) was measured by a two-site immunoradiometric assay, which detects PTHrP 1-74 (Nichols Institute).

Statistical methods. Results are expressed as mean ± the SE. The data were analyzed by using Prism software (GraphPad Software, Inc.) by repeated-measures analysis of variance. A P value of <0.05 was considered significant.

RESULTS

Ras^{V12} effector pathways promote tissue specific metastasis. A large number of growth factor receptors and their ligands are upregulated in advanced prostate cancer. It is possible that a common intermediary in growth factor-mediated signaling pathways contributes to prostate cancer progression. The Ras GTPase is a convergence point in growth factor receptor signaling. Three Ras downsteam effectors known to play major roles in cellular transformation are the Raf, PI3K, and RalGEF proteins (32). Single amino acid substitutions in the effector loop region of Ras have been widely used to address the individual roles of these pathways. Ras^{V12} with the mutations T35S, Y40C, and E37G binds to and activates primarily Raf, PI3K, and Ral-GEF, respectively, although other potential effectors are known to bind as well (33, 43). DU145 is a cell line derived from a human prostate adenocarcinoma brain metastasis and contains wild-type Ras alleles (15, 37). DU145 is tumorigenic in immunocompromised mice but has low experimental metastasis activity (7, 26). To investigate whether Ras-initiated signaling pathways promote prostate cancer metastasis, DU145 cells were infected with retroviruses expressing constitutively active H-Ras^{V12} or one of the three H-Ras^{V12} effector mutants (referred to hereafter as Ras). The expression of Ras in the various populations is shown in Fig. 1A. The relative expression level of Ras was similar in the effector mutants DU145Ras^{V12S35}, Ras^{V12G37}, and Ras^{V12C40} and was notably higher than that observed in cells infected with EV. Ras^{V12}-infected populations demonstrated only slightly increased levels relative to EV-infected cells, although comparable infections of other human epithelial cell lines demonstrated substantial Ras^{V12} overexpression. DU145 cells were independently infected twice with Ras^{V12} viruses, which resulted in populations expressing low levels of Ras, suggesting that selection against high Ras^{V12} expression had occurred. We evaluated the activation of downstream signaling pathways in the various cell lines (Fig. 1A) utilizing phospho-ERK1/2 and AKT as indicators of the Raf and PI3K pathways, respectively. RalGEF function was measured by determining the level of its enzymatic product, RalA-GTP, using a pull-down assay. Activation of the Raf/mitogen-activated protein kinase pathway was observed in DU145Ras^{V12} and Ras^{V12S35} populations, as well as a small increase in DU145Ras^{V12C40} cells. Increased RalGEF signaling was seen in DU145Ras^{V12} and

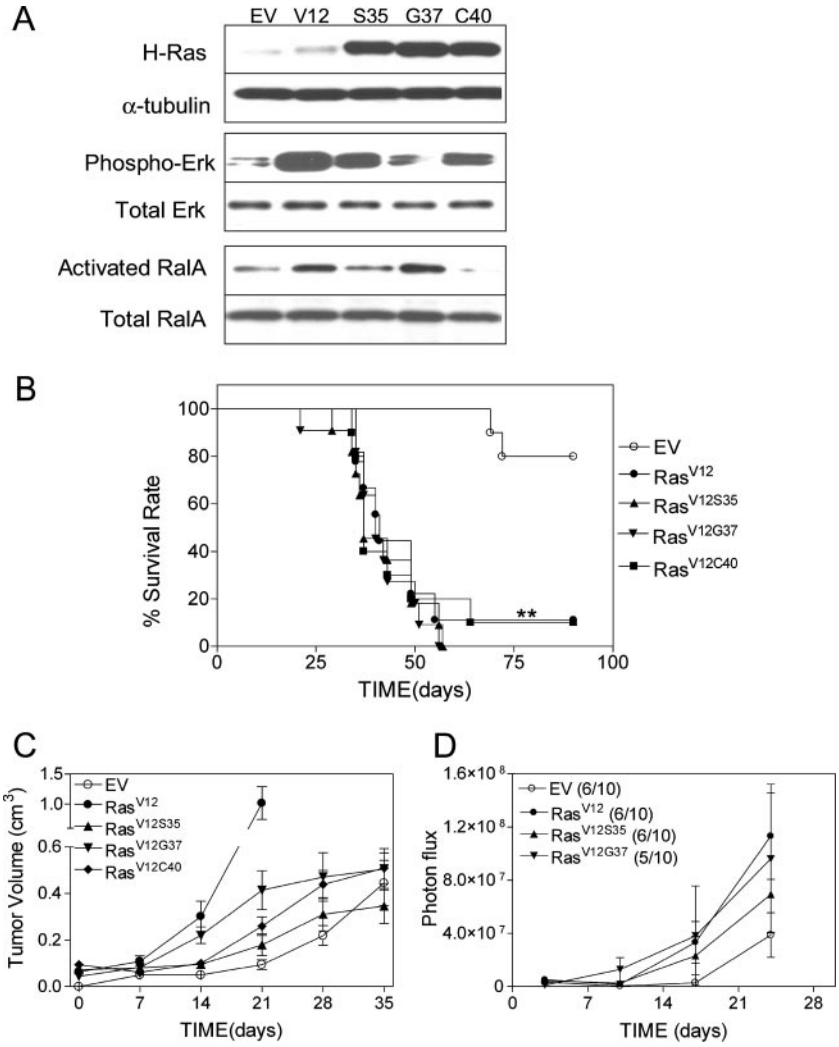

FIG. 1. Oncogenic Ras and Ras effector mutants activate the metastatic potential of DU145 cells. (A) Western blot analysis showing H-Ras, phosphorylated Erk and activated RalA expression in DU145 cells expressing different Ras mutants. α-Tubulin, total Erk, and total RalA served as loading controls, respectively. Proteins in whole-cell lysates were separated by sodium dodecyl sulfate-polyacrylamide gel electrophoresis. Activated RalA was measured by detecting RalBP1-bound RalA after immunoprecipitation. (B) Kaplan-Meier curve showing the survival rate of mice bearing different DU145 cell lines. Mice were sacrificed after 10% loss of body weight, paraplegia, imbalance, or head twisting. The data represent the percent survival versus time (days). **, $P < 0.01$ as determined by log-rank test compared to the DU145EV control group. There were no significant differences between DU145Ras^{V12} and DU145Ras^{V12} effector mutant groups. $n = 10$ to 12 mice per group. (C) Tumor growth rate in vivo after subcutaneous injection of DU145Ras^{V12} and different Ras effector mutants. The data represent the tumor volume (cm^3) ± the SE versus time (days). $n = 10$ tumors per group. (D) Tumor growth rate in bone after intratibial injection. The data represent average photon flux ± the SE over time. $n = 10$ tibiae per group. Number of tibia that developed tumors in bone is indicated in parentheses. No significant differences were detected by using two-way analysis of variance ($P > 0.1$).

Ras^{V12G37} cells, as shown for the RalA isoform. In addition to establishing the expected specificity of the Ras^{V12S35} and Ras^{V12G37} effectors, these results show that although Ras^{V12} levels were not markedly increased above endogenous Ras, there was potent activation of downstream pathways.

Contrary to expectations for an activated PI3K pathway, DU145Ras^{V12C40} cells did not show enhanced AKT phosphorylation on either T308 or S473 nor on downstream targets of AKT, including GSK-3β, p70S6K, or FOXOA3 (not shown). DU145 cells express wild-type PTEN, which downregulates PI3K activity. After serum stimulation of DU145 cells, we observed weak phosphorylation of AKT that was severalfold reduced compared to similarly stimulated samples of LnCaP prostate tumor cells, which have lost PTEN expression. Either due to PTEN expression or other unknown factors, it appears that DU145 cells do not maintain sustained activation of AKT. However, despite a lack of AKT activation, we found that DU145Ras^{V12C40} cells were functionally modified with respect to metastasis (see below).

The metastatic properties of DU145 cells expressing activated Ras or Ras effector pathways were evaluated in an experimental metastasis assay, which reflects the arterial distribution of injected cells to multiple organs via left ventricle inoculation. This model measures several steps in the metastatic process, including survival in the circulation, extravasation, and colonization of tumor cells in different organs. A

TABLE 1. Metastasis development in various organs

Cell line (no. of mice tested)	Absolute no. of mice (%)[a]				
	Long bones	Spine	Brain	Adrenal glands	Kidney
DU145/EV (10)	0 (0)	0 (0)	0 (0)	0 (0)	0 (0)
DU145/Ras^{V12} (12)	8 (67)	3 (30)	8 (67)	4 (33)	0 (0)
DU145/Ras^{V12S35} (10)	4 (40)	3 (30)	8 (80)	4 (40)	1 (10)
DU145/Ras^{V12G37} (11)	10 (91)	3 (27)	3 (27)	2 (18)	0 (0)
DU145/Ras^{V12C40} (10)	3 (30)	0 (0)	8 (80)	3 (30)	0 (0)

[a] Shown are the absolute number and percentage of mice that developed metastasis in the indicated organ. An animal with any detectable tumor growth in the indicated organ was scored as positive, and thus the numbers in the table do not indicate metastatic burden. Metastatic burden is indicated in Fig. 2C and Fig. 3C and D. Mice were euthanized between 6 and 9 weeks after tumor cell inoculation.

Kaplan-Meier plot of survival for mice inoculated with DU145 containing EV, Ras^{V12}, or the various effector mutants is shown in Fig. 1B. Most of the mice bearing DU145EV cells survived more than 3 months, while the majority of mice bearing DU145Ras^{V12,} Ras^{V12S35}, Ras^{V12G37}, or Ras^{V12C40} died between 6 and 8 weeks with evidence of weight loss and neurological or skeletal complications. Necropsies to determine the cause of death revealed dramatic differences in the tissue specificity of metastasis, with obvious bone metastasis caused by DU145Ras^{V12} and Ras^{V12G37} cells, and brain metastasis caused by DU145Ras^{V12}, Ras^{V12S35}, and Ras^{V12C40} cells (Table 1). A moderate and similar degree of adrenal gland metastasis was observed with all cell lines except the DU145EV.

To evaluate the contribution of tumorigenic growth to the metastatic properties of the various cell lines, in vitro and in vivo growth assays were performed. The in vitro growth rate of the DU145 lines expressing Ras^{V12}, Ras^{V12S35}, Ras^{V12G37}, and Ras^{V12C40} was similar and slightly greater than the parental DU145 line (not shown). Inoculation of the various cell lines subcutaneously (Fig. 1C) revealed that the DU145/Ras^{V12} cells produced the largest and most rapidly growing tumors, necessitating euthanasia of the mice by 3 weeks. DU145Ras^{V12S35}, Ras^{V12C40}, Ras^{V12G37}, and EV cells formed tumors of similar sizes by 5 weeks, and the DU145Ras^{V12G37} cells appeared to have a faster initial growth rate. Finally, intratibial growth was assessed with DU145 cell lines carrying a bioluminescent reporter, a fusion protein composed of herpes simplex virus type 1 thymidine kinase, GFP, and luciferase domains (TGL), in addition to Ras^{V12} or its effector mutants (30). All of the cell lines demonstrated similar GFP fluorescence upon fluorescence-activated cell sorting analysis and similar levels of ex vivo luciferase activity (not shown). All Ras-expressing cell lines grew well in the bone marrow and demonstrated approximately the same rate of growth, measured as photon flux, with DU145EV being the slowest. There was no significant difference in the percentage of mice that developed bone tumors in comparing the DU145Ras^{V12}, EV, and effector mutant lines (Fig. 1D). All tumors were osteolytic as determined by histology and X-ray imaging (not shown).

Ras^{V12S35} and Ras^{V12C40} mediate brain metastasis. Animals inoculated with DU145Ras^{V12}, Ras^{V12S35}, and Ras^{V12C40} expressing lines developed multiple brain metastasis in ca. 67, 80, and 80%, respectively, of the mice examined (Table 1 and Fig. 2). Mice within these experimental groups often displayed weight loss, deformed calvaria, and ataxic movement or other neurological abnormalities. As shown in Fig. 1B, the time to severe morbidity for 50% of the animals was 5 weeks, and 95% of the animals did not survive beyond 8 weeks. In contrast, DU145Ras^{V12G37}-transformed cells formed brain metastasis at a low frequency (27%). DU145EV cells did not form brain metastasis in the time frame which resulted in morbidity in the other groups, but rare small tumors were observed in mice evaluated 6 months after inoculation. Most brain metastases were observed throughout the various regions of the cortex and occasionally in the cerebellum or olfactory bulbs (Fig. 2A). Macroscopic metastases were visible between 2 and 3 weeks. Histological analyses revealed that DU145Ras^{V12S35}, Ras^{V12C40}, and Ras^{V12G37} metastases grew in dispersed, infiltrative clusters of cells, whereas DU145Ras^{V12} tumors grew as solid, vascularized masses (Fig. 2B). Figure 2C shows the average number of brain metastases per mouse in each group. DU145Ras^{V12}-, DU145Ras^{V12S35}-, and DU145Ras^{V12C40}-injected mice presented with an average of three to four brain tumors per mouse. However, DU145Ras^{V12G37} bearing mice presented with an average of less than one brain tumor per mouse. In summary, the Ras^{V12S35} and Ras^{V12C40} pathways significantly stimulated the colonization and growth of DU145 cells in the brain. In addition, the expression of fully functional activated Ras appeared to enhance angiogenesis.

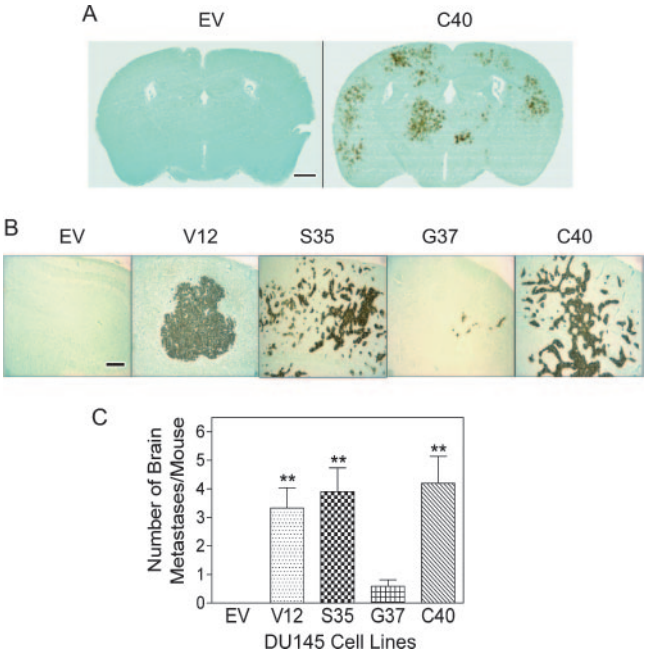

FIG. 2. Brain metastasis formed by DU145Ras^{V12} and different DU145Ras effector mutants. (A) Low-power micrograph of brain sections showing the distribution of multiple brain metastases in DU145Ras^{V12C40}-bearing mice compared to that of DU145EV control mice. Bar, 1 mm. (B) Representative histological sections of brain metastases from mice bearing DU145Ras^{V12} and the different Ras effector mutants. Cytokeratin 18-positive tumor cells (brown) in brain as revealed by immunohistochemical staining (50X) are shown. Bar, 200 μm. (C) Number of brain metastasis per mouse in each group quantified by using histological sections. Animal survival was as shown in Fig. 1B, and the final specimens were collected by 10 weeks. $n = 10$ to 12 mice per group. **, $P < 0.01$.

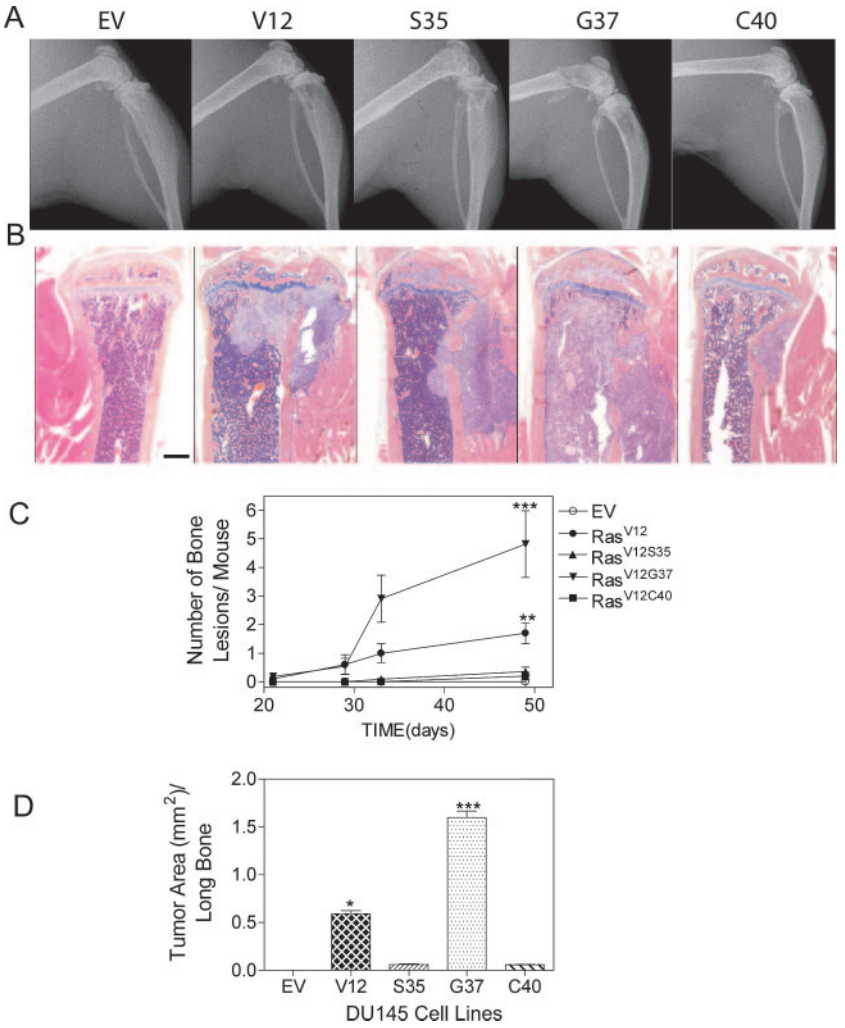

FIG. 3. Ras and Ras effector mutant-induced bone metastasis. (A) Representative radiographs of hind limbs from mice injected with various DU145 populations via an intracardiac route. Bone destruction was obvious in DU145Ras^{V12} and DU145Ras^{V12G37} groups compared to DU145EV, DU145Ras^{V12S35}, and DU145Ras^{V12C40} groups. (B) Representative histological sections of tibia from mice bearing different DU145 cell lines. Tumor has replaced the bone marrow cavity in the DU145Ras^{V12G37} group. Massive bone destruction and large tumor burdens were seen in the DU145Ras^{V12} group. Relatively small tumors and less bone destruction were evident in the DU145Ras^{V12S35} and DU145Ras^{V12C40} groups. No tumor cells were evident in the DU145EV group. Bar, 1 mm. (C) Number of bone lesions quantified on radiographs versus time (days). **, $P < 0.01$; ***, $P < 0.001$ (versus DU145EV control). (D) Histomorphometric analysis of tumor area in the long bones from different groups. *, $P < 0.05$; ***, $P < 0.001$ (versus DU145EV control).

Ras^{V12G37} mediates bone metastasis. DU145Ras^{V12G37}-bearing mice developed detectable osteolytic bone metastasis by 5 weeks in 90% of the mice examined, as determined by X-ray imaging (Fig. 3A). Each animal displayed multiple lesions, averaging five lesions per animal (Fig. 3C). Mice inoculated with DU145Ras^{V12} cells developed bone lesions in 75% of the animals, but the average number of lesions per animal was half that of animals bearing DU145^{V12G37} cells (Fig. 3A and C). Bone metastasis was infrequent in DU145Ras^{V12S35}- or Ras^{V12C40}-bearing animals. DU145Ras^{V12} and Ras^{V12G37} tumors were large and often filled the bone marrow cavity, whereas DU145^{V12S35} and Ras^{V12C40} tumors were usually smaller and grew more slowly (Fig. 3B). A histomorphometric analysis of tumor area per long bone is shown in Fig. 3D, demonstrating that DU145Ras^{V12G37} tumors grew approximately three times larger than DU145Ras^{V12} tumors and 20 times larger than DU145Ras^{V12S35} or Ras^{V12C40} tumors.

Bone metastasis was observed in long bones and vertebral bodies (Fig. 3A and B and see Fig. S1 in the supplemental material), the latter frequently resulting in spinal cord involvement and hind limb paresis. Vertebral bodies are common sites of prostate cancer metastasis in patients. The site of metastasis for the various cell lines was the periosteal surface (Fig. 3B). Cortical bone metastasis is most commonly observed in lung cancer patients and less so in breast cancer and other solid cancer types, where bone metastasis invasion usually begins on the endosteal surface (22). Metastases were predominantly osteolytic with reactive new bone formation in some tumors (see Fig. S1 in the supplemental material). Histological sections revealed frequent osteoclasts along the uneven periphery of the expanding tumors.

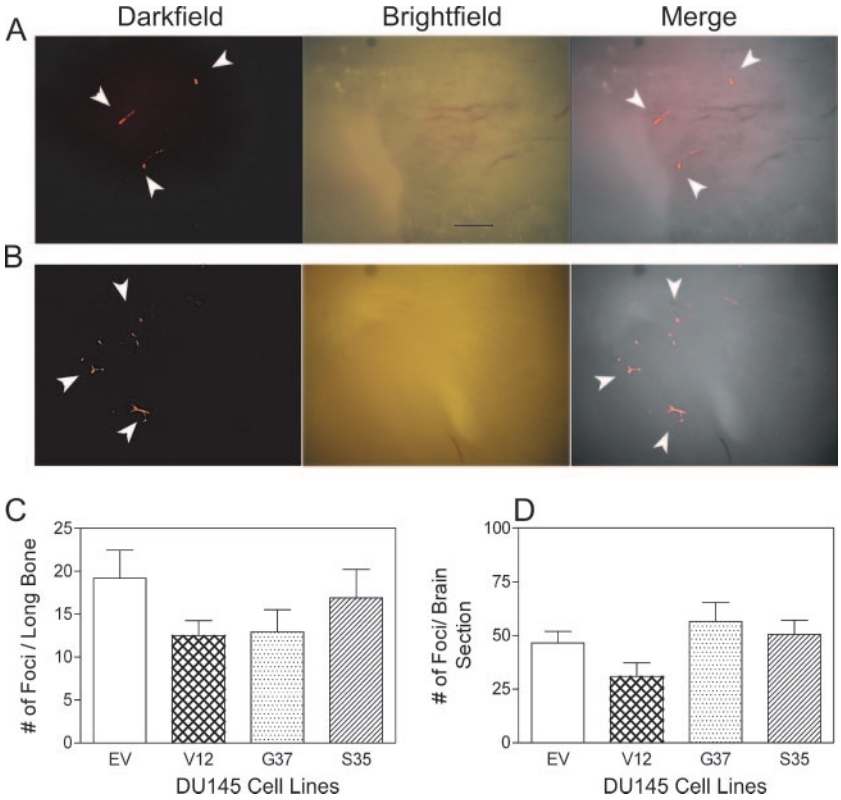

FIG. 4. Quantification of tumor cells arrested in the vasculature of brain and bone. (A) Fluorescent cells indicated by the arrows are shown on the surface of a tibia as visualized by using fluorescence stereomicroscopy. Bar, 100 μm. (B) Fluorescent cells in a brain section. (C) Average number of foci per bone for DU145EV, DU145Ras^{V12}, DU145Ras^{V12G37}, and DU145Ras^{V12S35}. Four bones were counted from each mouse. (D) Average number of foci per brain section for various DU145 derivative cell lines. Four sections were counted from each mouse. $n = 3$ mice per group. No significant differences were detected by using one-way analysis of variance ($P > 0.05$).

Interestingly, although bone metastases were significantly less frequent and smaller for DU145Ras^{V12S35} or DU145Ras^{V12C40} compared to DU145^{V12G37}, there was no obvious difference in the histology of various tumors (Fig. 3B and data not shown). The localization of the tumors and their osteolytic nature appeared similar among the various effector pathway-expressing cell lines. Conditioned media from the various cell lines stimulated similar degrees of bone marrow-derived osteoclast maturation in vitro (see Fig. S2 in the supplemental material). In addition, direct measurements of secreted PTHrP, a factor known to play a significant role in tumor-mediated osteoclastogenesis (14), was similar in the various cell lines (results not shown).

Ras effector pathways do not influence the distribution of tumor cells within various organs after hematogenous dissemination. An important question to consider with respect to the organ tropism of the DU145 cell lines is whether the various Ras signaling pathways influence homing or organ distribution after hematogenous spread. To visualize distribution patterns of the bulk of cells over time, we analyzed the various TGL-expressing DU145 cell lines by using BLI immediately and at 1, 7, 12, or 20 days postinoculation (see Fig. S3 in the supplemental material). All cell lines demonstrated similar patterns of organ distribution within the first week, which showed high levels within the brain and kidneys at day 1 and loss of the majority of signal by day 7. There was evidence of the expected organ-specific patterns of metastasis starting at day 12. Thus, the distribution of the bulk of injected cells and their survival over time was similar for the various cell lines.

In order to quantify the distribution of single cells in specific organs after hematogenous dissemination, the DU145 cell lines were labeled in vitro with SNARF-1, a stable cell-permeable fluorescent probe, prior to inoculation. Five hours later, tissues were collected and individual cells were counted by using a fluorescent stereomicroscope. Because DU145 cell derivatives initiate bone metastases from the cortical surface, the surfaces of bones from the hind limbs were analyzed (Fig. 4A). The adrenal gland and sections of brain and kidney, prepared at uniform thickness and spatial position, were also analyzed. The majority of cells were lodged in capillaries (note the shape of the tumor cells deformed within the capillaries in Fig. 4A and B). The absolute numbers of cells from the DU145 cell lines that were localized to bone (Fig. 4C), brain (Fig. 4D), kidneys, or adrenal glands (not shown) did not vary significantly. We conclude that the expression of oncogenic Ras or Ras effector pathways does not alter the distribution of DU145 cells relative to the organs that develop metastasis.

The RalGEF pathway is necessary and sufficient to mediate bone metastasis. Bone is the most common site of prostate cancer metastasis, occurring in more than 80% of patients with progressive disease. Therefore, we sought to determine the underlying signaling pathway responsible for the dramatic bone metastasis phenotype of the DU145Ras^{V12G37} cell pop-

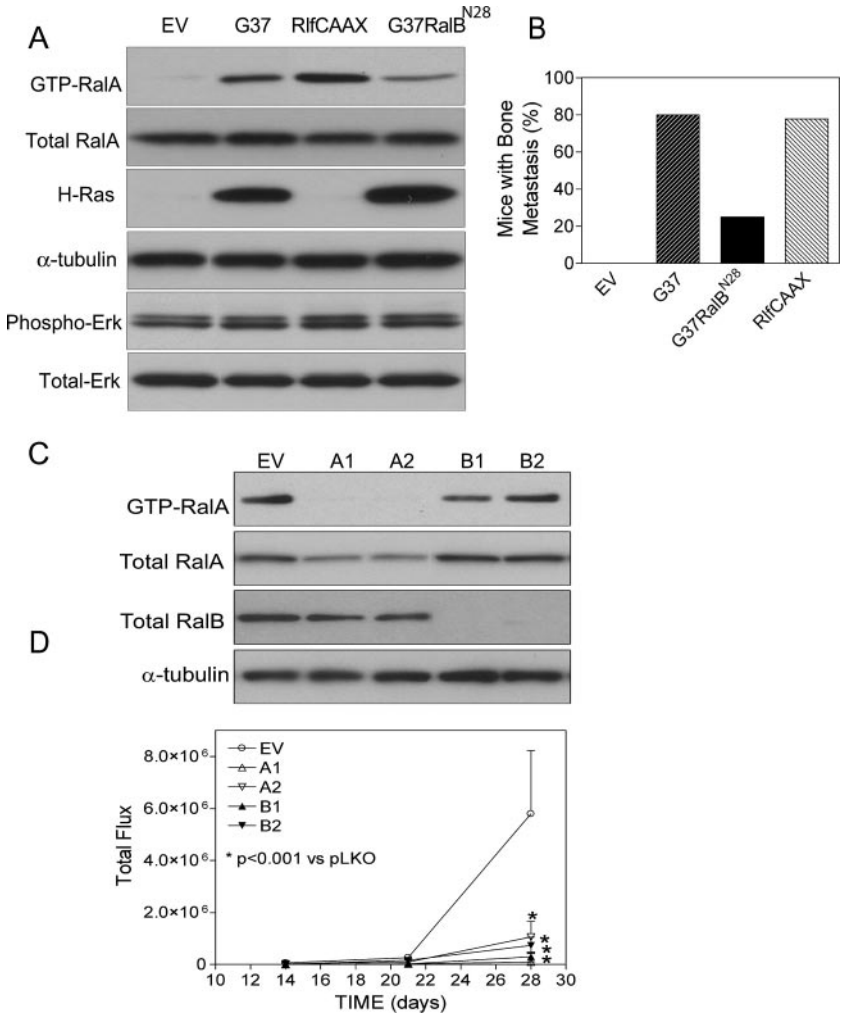

FIG. 5. Activation of RalGEF pathway is necessary and sufficient for the development of bone metastasis by DU145 cells. (A) Immunoblot analysis of Ras, activated RalA, and phosphorylated Erk expression in DU145EV, DU145Ras^{V12G37}puro, DU145RlfCAAX, and DU145Ras^{V12G37}RalB^{N28} cell lines. Activated RalA was measured by detecting the RalBP1-bound RalA after immunoprecipitation. α-Tubulin, total RalA, and total Erk were used as loading controls. (B) Percentage of mice that developed bone metastasis 6 weeks after intracardiac injection. $n = 10$ to 12 mice per group. (C) Immunoblot analysis of RalA and RalB levels in DU145Ras^{V12G37} after introduction of shRNAs. RalA shRNAs are labeled A1 and A2, and RalB shRNAs are labeled B1 and B2. α-Tubulin is used as a loading control. (D) RalA and RalB are required for metastatic tumor growth in bone. DU145Ras^{V12G37} cells expressing the aforementioned shRNAs against RalA and RalB were injected via the intracardiac route. Metastatic tumor growth was monitored via BLI. The line graph shows the average photon flux per animal per group over a 4-week period. $n = 8$ mice per group. The total numbers of metastases at week 28 were as follows: PLKO ($n = 7$), RalAshRNA1 ($n = 2$), RalAshRNA2 ($n = 2$), and RalBshRNA1 ($n = 3$), RalBshRNA2 (5). *, $P < 0.05$ versus EV control.

ulation. The activity of the Ras^{V12G37} effector pathway is generally attributed to activation of RalGEFs, but this effector domain mutant does interact with other proteins. To determine whether RalGEF activity is sufficient, we introduced a membrane-associated, constitutively active RalGEF, RlfCAAX, into DU145 cells. RalA-GTP levels were quantified by utilizing a RalBP1 pull-down assay, which demonstrated stimulation to a level greater than the Ras^{V12G37} (Fig. 5A). After left ventricle inoculation, the development of bone metastasis was monitored by X-ray and histological analyses in injected mice. DU145RlfCAAX cells developed osteolytic bone metastasis in long bones and vertebral bodies similarly to DU145Ras^{V12G37} cells, demonstrating that an activated RalGEF can substitute for the Ras^{V12G37} effector pathway in this assay (Fig. 5B). To determine whether RalGEF activation is essential for the bone metastatic activity of DU145Ras^{V12G37} cells, a dominant-negative approach was used by expressing RalB^{N28}. RalB^{N28} forms a nonproductive complex with RalGEFs, resulting in reduced levels of total GTP-bound Ral (Fig. 5A). Basal phospho-ERK levels were used as a control and were found to be unaffected by RlfCAAX or RalB^{N28} expression. RalB^{N28} had no effect upon the in vitro growth of DU145Ras^{V12G37} but did appear to mildly suppress subcutaneous growth of DU145Ras^{V12G37} (data not shown). Figure 5B shows that the ability of DU145Ras^{V12G37}RalB^{N28} cells to develop bone metastasis was reduced by ca. 65% compared to DU145Ras^{V12G37}puroEV.

RalGEFs stimulate GTP exchange on two substrates, RalA and RalB. To determine which Ral isoforms are necessary for bone

metastasis formation, luciferase-expressing DU145Ras^{V12G37} (DU145Ras^{V12G37}/TGL) cells were infected with lentiviruses encoding shRNAs directed against either RalA or RalB. Two distinct shRNAs against RalA (A1 and A2) and RalB (B1 and B2) were used, and protein knockdown in resultant lines is shown in Fig. 5C. Luciferase activity per cell was similar in the various cell lines (not shown).

DU145Ras^{V12G37}/TGL cells infected with the EV or the derivative knockdown populations were injected via the left cardiac ventricle, and metastasis formation was monitored by BLI over time. As shown in Fig. 5D, there was a significant decrease in the development of bone metastasis by cell lines with either reduced RalA or reduced RalB compared to EV-infected cells. Reduced total photon flux resulted from an ca. 50% decrease in tumor initiation coupled with a two- to three-fold decrease in tumor growth (see Fig. 5 legend). In addition, we observed what appeared to be a regression of two independent vertebral metastases in each of the RalA and RalB knockdown groups, totaling four in all (data not shown). In contrast, no such regression was observed in the control group, nor has it been a common observation for DU145Ras^{V12G37}/TGL cells in independent experiments. All mice inoculated with DU145Ras^{V12G37}/TGL-pLKO EV-infected cells required euthanasia at day 28. Mice inoculated with cells in which RalA or RalB had been knocked down were healthy at day 28. Importantly, reduction of RalA, but not RalB, decreased subcutaneous tumorigenesis of DU145Ras^{V12G37}/TGL cells (see Fig. S4 in the supplemental material), a finding consistent with other published data for Ras-activated cell lines expressing shRNA against RalA (18). We conclude that activation of both RalA and RalB is required for the bone metastatic activity that is stimulated by Ras^{V12G37}, although dissecting a role for RalA in metastasis is complicated by its role in tumorigenesis.

To complement these results, we attempted to mimic the bone metastatic activity of RlfCAAX (Fig. 5B) by introducing constitutively activated forms of RalA, RalA^{V23}, RalB, and RalB^{V23}, either separately or together, into DU145 cells. Although we obtained DU145 cells expressing significantly elevated levels of GTP-bound RalA and/or RalB, neither activated isoform alone nor both together significantly increased the bone metastatic activity of the DU145/TGL parental cell line (not shown), suggesting that RlfCAAX may have additional functions beyond GTP exchange activity. Another possibility is that constitutively GTP-bound Ral isoforms do not mimic the cycling exchange of GTP mediated by RlfCAAX. Taken together, these data suggest that RalA and RalB activation is necessary but not sufficient for bone metastasis downstream of Ras^{V12G37}.

Finally, CD24, which has been identified as a RalA/B-dependent target in bladder cancer cells, was of specific interest in the DU145 model because it has been suggested that CD24 plays a role in metastasis as a result of its affinity for P-selectin, leading to the formation of microemboli that lodge in secondary organs (6). However, we have determined that the various oncogenic Ras effector mutants induce CD24 surface expression in DU145 cells to equivalent degrees, suggesting that CD24 may contribute to metastatic ability but is not a unique determinant of tissue-specific colonization (results not shown).

Loss of RalA leads to inhibition of growth in bone by metastatic PC3 cells. To address the general requirement for RalA or RalB-mediated signaling pathways in prostate cancer bone metastasis, we expanded our analysis to the PC3 cell line, which was originally isolated from a prostate cancer bone metastasis. PC3 has wild-type Ras alleles, is highly metastatic to bone in xenograft assays, and is a widely used model of prostate cancer bone metastasis (15). Consistent with the hypothesis that Ral-GTP levels contribute to growth of prostate cancer in bone, bone metastatic parental PC3 cells demonstrated approximately four to five times more GTP-bound RalA relative to total Ral than the weakly metastatic DU145 parental cells (not shown). Lentivirus-encoded shRNAs directed against RalA and RalB were introduced into TGL-expressing PC3 cells, and the metastatic and tumorigenic potentials of these cells were analyzed. As shown in Fig. 6A, two distinct RalA shRNAs (A1 and A2) decreased RalA protein levels by ~3-fold compared to the EV control. Measurement of RalA-GTP by immunoprecipitation using RalBP1 showed that activated RalA was knocked down by ~5-fold in the presence of RalA-directed shRNA. The RalB-directed shRNAs B1 and B2 reduced RalB protein levels sixfold and to nondetectable levels, respectively. RalB-GTP levels were not detectable. Consistently we observed increased RalA levels in cell populations with decreased RalB (Fig. 6A). Importantly, all cell populations had similar levels of luciferase activity ex vivo (see Fig. S5A in the supplemental material). All cell lines grew at similar rates in vitro (data not shown). Tumorigenic potential was assayed by evaluating subcutaneous tumor growth (see Fig. S5B in the supplemental material). Tumors arising from the various cell lines described above grew to similar sizes and at similar rates. Cells isolated and expanded from tumors demonstrated comparable reductions in Ral proteins as the starting populations of inoculated cells, as shown for RalA in Fig. 6D.

The metastatic characteristics of PC3 cells with reduced RalA or RalB levels were analyzed after inoculation via the left cardiac ventricle. Mice were imaged for bioluminescence after inoculation and then once per week starting at week 3. Mice inoculated with EV or RalB knockdown cells developed signs of extreme morbidity at weeks 6 to 7, and the experiment was terminated to allow histological comparison of equivalently aged tumors. The data in Table 2 show the number of tumors detectable by bioluminescence at various anatomic sites over time. PC3 and derivative cell populations exhibited a dominant tropism to bone, including the jaw, long bones, and vertebral bodies, and rarely to the adrenal glands. Bioluminescence signals were not apparent until 3 weeks postinoculation. An analysis of tumor numbers and growth over time clearly demonstrated a greatly reduced metastatic potential for both PC3/A1 and PC3/A2. At week 3, signals were apparent in the jaws of at least half of the animals in each experimental group. By week 6, the numbers of detectable tumors in the jaw were similar or slightly decreased for most groups except the PC3/A1 line, where the majority of tumors could no longer be detected. In addition, PC3/A1 developed no and PC3/A2 developed fewer long bone and vertebral metastases compared to the other groups. Importantly, quantification of photon flux over time for all bone tumors showed that the EV control, PC3/EV, and the RalB knockdown lines, PC3/B1 and PC3/B2, increased dramatically, ~1,000-fold between weeks 3 and 6 (Fig. 6B). In

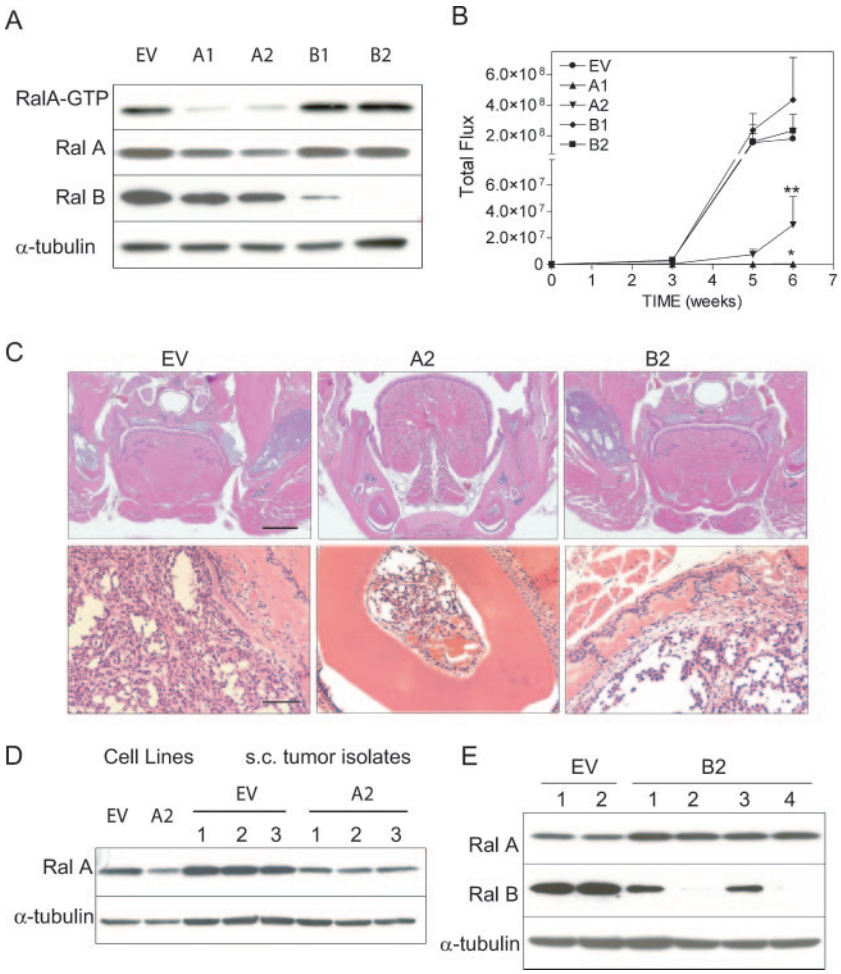

FIG. 6. Reduced RalA inhibits metastasis of PC3 cells to bone. (A) Detection of RalA or RalB by Western blot analysis in PC3 cells stably expressing RalA shRNA (A1 and A2) or RalB shRNA (B1 and B2) or in the EV control. α-Tubulin serves as a loading control. (B) RalA is required for metastatic tumor growth in bone. PC3 cells expressing the aforementioned shRNAs against RalA and RalB were injected via the intracardiac route. Metastatic tumor growth was monitored via BLI. Line graph shows the average photon flux per animal per group over a 6-week period. $n = 8$ to 15 mice per group. RalA shRNA bearing mice exhibited significantly less tumor burden in the bone than EV control mice and RalB shRNA-bearing mice. *, $P < 0.05$; **, $P < 0.01$ (versus EV control). (C) Representative histological sections with hematoxylin and eosin staining of sectioned mandibles taken from mice injected with the indicated cells. Bars: top panel, 50 μm; lower panel, 10 μm. Large osteolytic tumor masses can be seen in the jaws of EV control and RalB shRNA-bearing mice, replacing bone marrow, destroying adjacent bone, and growing out into the surrounding soft tissue. In contrast, tumor cells are rarely observed in the jaw bone marrow cavities of RalA shRNA-bearing animals; occasionally, tumor cells are found in tooth root compartments, as shown. (D) Immunoblot analysis of RalA levels in cells isolated from subcutaneously grown tumor (s.c. tumor isolates) and cell lines not passaged though animals (cell lines). Tumors were isolated from mice injected with the indicated cell line and expanded in vitro. An immunoblot shows RalA levels in three EV control tumors and four RalA shRNA-expressing tumors. Tubulin is used here as a loading control. (E) Immunoblot analysis of RalA and RalB levels in cells isolated from jaw and long bones of mice injected via the intracardiac route with the indicated cell lines. Tumors were isolated from mice and expanded in vitro. Tubulin is used here as a loading control.

contrast, there was virtually no growth of bone metastases for PC3/A1 and only a 10-fold increase for PC3/A2.

A portion of organs displaying bioluminescence signal were analyzed histologically from each experimental group. Osteolytic tumors typical of PC3 cells were identified in the majority of evaluated PC3/EV, PC3/B1, and PC3/B2 inoculated mice (Fig. 6C). In addition, it was not uncommon to observe clusters of tumor cells in tooth pulp adjacent to mandible tumors. In contrast, visible bone tumors were found in only zero of four or two of six bioluminescence signal-positive organs from PC3/A1 and PC3/A2 inoculated mice, respectively, although occasionally tumor cell clusters in the tooth pulp were observed. Because the organs were not exhaustively sectioned, we expect the existence of small tumors outside the sections that were collected as suggested by the presence of bioluminescence signals.

To determine whether bone tumors derived from shRNA-expressing populations initiated from cells that had escaped knockdown, tumor cells were isolated and selectively grown in culture from bioluminescence-positive organs, expanded in tissue culture in the presence of puromycin, and analyzed for RalA and RalB levels. Only one cell line, which subsequently did not thrive, was derived from PC3/A2 tumors. Several cell lines were derived from RalB knockdown tumors, and repre-

TABLE 2. PC3 metastasis development in various organs

Cell line (no. of mice tested)	Absolute no. of mice (%)[a]				
	Jaw (wk 3)	Jaw (wk 6)	Long bones (wk 6)	Spine (wk 6)	Adrenal glands (wk 6)
PC3/EV (15)	12 (80)	9 (60)	5 (33)	2 (13)	0 (0)
PC3/A1 (9)	8 (89)	1 (13)	0 (0)	0 (0)	0 (0)
PC3/A2 (8)	7 (88)	5 (63)	2 (25)	0 (0)	2 (25)
PC3/B1 (8)	5 (63)	6 (75)	4 (50)	1 (13)	2 (25)
PC3/B2 (9)	5 (56)	5 (56)	3 (33)	3 (33)	2 (22)

[a] Shown are the absolute numbers and percentages of mice that developed metastasis in the indicated organ at week 6. An animal with detectable bioluminescent signal in the indicated organ for at least two consecutive weeks was scored as positive, and thus the numbers in the table do not indicate metastatic burden. Metastatic burden is indicated in Fig. 6B. Also shown are absolute numbers and percentages of animals with jaw tumors visible at weeks 3 and 6. Mice were euthanized at 7 weeks after tumor cell inoculation. Representative organs displaying bioluminescence signals were analyzed histologically. Adrenal gland and spine metastases were confirmed, as were the majority of jaw and long bone metastases, although some organs were used to culture metastatic tumors.

sentative examples are shown in Fig. 6E. In all of these bone tumor-derived cell lines, RalB protein was lower than that in PC3/EV tumor-derived lines. Individual tumor-derived lines expressed variable levels, indicating clonal variation, but a comparison of RalB protein levels and tumor size did not reveal any correlation (data not shown). Interestingly, RalA protein levels were uniformly increased, as was observed in the cell lines prior to passage through animals. From the combined analysis of bioluminescence signal over time, pathological evaluation, and selection for tumor-derived cell growth in vitro, we conclude that a reduction of RalA but not RalB levels in PC3 cells significantly inhibited the development of bone metastasis.

To analyze whether RalA-dependent bone growth is tumor type specific, RalA and RalB knockdown experiments were performed with the MDA-MB-231 breast cancer cell line, which contains mutant oncogenic Ras. After cardiac inoculation, the development of bone metastasis with respect to site, number, and kinetics of growth was determined by using BLI. There was no significant effect of RalA or RalB knockdown on tumorigenesis or metastasis development by MDA-MB-231 (see Fig. S6A in the supplemental material). Loss of RalA and RalB was verified in growing metastases (see Fig. S6B in the supplemental material). Therefore, we conclude that the requirement for RalA may vary with tumor type, and the inhibition of bone metastasis associated with RalA loss in prostate cancer cell lines is not simply secondary to a generalized or nonspecific growth inhibition.

DISCUSSION

As pleiotropic regulators, signaling pathways that underlie tissue-specific survival and growth of metastases are desirable therapeutic targets. Because elevated growth factor receptor signaling is a common progression factor in prostate cancer, we evaluated the function of Ras-dependent signaling pathways, which are downstream of such receptors, in prostate cancer metastasis. DU145, a prostate cancer cell line with low metastatic potential, was used to demonstrate in a xenograft experimental metastasis model that activated Ras signaling promotes metastasis in multiple tissues, including bone. Remarkably, the expression of Ras-mediated effector pathways differentially stimulated metastasis in different organs, which did not result from obvious differences in tumorigenic growth properties of the various lines. Ras^{V12S35} and Ras^{V12C40} pathways activated brain metastasis formation, while Ras^{V12G37} expression induced bone metastasis. The DU145 cell line was initially isolated from a brain metastasis, and therefore it was not unexpected that these cells displayed tropism for the brain (37). It was somewhat more surprising that the overexpression of the RalGEF effector pathway was able to redirect colonization to the bone, the most common site of advanced prostate cancer metastasis. These data directly demonstrate that the ability of DU145 tumor cells to grow in distinct microenvironments is supported by activation of different signaling pathways.

A role for the Ral pathway in prostate cancer growth in bone is further supported by the loss of bone metastatic activity in PC3 cells that have shRNA-mediated decreases in RalA expression. The lack of effect of reduced RalA and RalB levels upon the tumorigenic potential of PC3 cells allowed us to evaluate the necessity of RalA and RalB for metastasis-specific functions. Metastasis-specific functions include homing, the initiation of clonal growth, and the transition to expansive growth after the development of micrometastases. The existence of weak and nonprogressing bioluminescent signals for many bone sites containing PC3 RalA knockdown cells implies normal homing and colonization by these cells without expansion of initiated tumors. Likewise, the regression of vertebral bioluminescent signals in either RalA or RalB knockdown DU145Ras^{V12G37} is consistent with Ral activity contributing to expansive growth in bone. In addition, we found no evidence upon direct observation of fluorescently labeled cells for homing differences among the various Ras effector-transformed DU145 cell lines.

The inhibition of growth in bone as a consequence of Ral pathway inactivation did not result from a nonspecific effect but instead appears to be cell line dependent. Neither RalA nor RalB knockdown in MDA-MB-231, which contains a K-Ras mutation, or colon cancer HT29 cells, which express wild-type Ras, inhibited the development of bone metastases after arterial inoculation (data not shown; see Fig. S6 in the supplemental material). The genetic background in which the Ral pathway contributes to bone growth presumably depends upon the variety of genomic alterations that drive tumorigenesis in individual cancers. In this regard, a requirement for both RalA and RalB in RasV12G37-mediated metastasis of DU145 cells parallels a previous report showing the necessity for both homologues in a lung colonization assay of pancreatic cancers (18). A total of 90% of pancreatic cancers harbor Ras mutations. In contrast, PC3 cells required RalA, but not RalB, for efficient growth in bone. PC3 cells are highly aggressive at establishing bone metastases, and we hypothesize that other pathways compensate for RalB in these cells.

Because cooperation with TGF-β is a function of Ras that is relevant to cancer progression (1) and TGF-β is expressed at high levels in bone matrix, we determined the sensitivity of the various cell lines to TGF-β-mediated growth inhibition. Interestingly, we found that DU145 parental cells were inhibited by TGF-β and that expression of the Ras^{V12S35} or Ras^{V12G37}

pathways relieved the TGF-β growth inhibition (results not shown). Therefore, cooperation with TGF-β may play a role in metastasis development by Ras effector pathway-transformed DU145 cells, but such cooperation does not account for tissue specific differences in the effector pathways. We are currently investigating a role for Ral in TGF-β responsiveness with regard to proteolytic activity and extracellular matrix degradation.

A function that is expected to stimulate tumor growth in bone is the production of factors that increase the activation and/or differentiation of osteoclasts, resulting in bone resorption and leading to the release of tumor-stimulating factors (24). Due to the aggressive breakdown of cortical bone in DU145Ras^{V12G37} metastases, there may be increased osteoclastogenesis associated with such bone tumor formation relative to the other derivative cell lines. However, if this is the case, it would appear that the mechanism of osteoclastogenic stimulation is not attributable to DU145Ras^{V12G37} cells alone, as judged by the relatively similar production of osteoclastogenic factors (see Fig. S2 in the supplemental material) compared to parental DU145. It is quite possible that the osteolytic activity of DU145Ras^{V12G37} cells is regulated by the bone microenvironment, perhaps resulting from interaction with matrix or cellular components that reside in the bone. Future investigations will address RalGEF-dependent microenvironment interactions.

At present, there are no robust mouse genetic models of prostate cancer metastasis to bone, the most common site of human prostate cancer metastasis. In addition, clinical specimens of prostate cancer bone metastases are not readily available, especially in a form that is amenable to molecular profiling or the direct measurement of enzymatic activity for most proteins. We have described two complementary models showing that the RalGEF/Ral pathway supports prostate cancer bone metastasis. Xenograft models such as these that make use of isogenic cell lines to address functional changes in the context of bone provide a comparative tool for identifying potential targets that mediate organ-specific growth.

ACKNOWLEDGMENTS

This research was supported by the Intramural Research Program of the NIH, National Cancer Institute, Center for Cancer Research.

We thank Ilona Linnoila for expert advice with reviewing histology and pathology. We thank Glenn Merlino and Chand Khanna for helpful suggestions.

REFERENCES

1. **Akhurst, R. J., and R. Derynck.** 2001. TGF-β signaling in cancer: a double-edged sword. Trends Cell Biol. **11:**S44–S51.
2. **Bakin, R. E., D. Gioeli, R. A. Sikes, E. A. Bissonette, and M. J. Weber.** 2003. Constitutive activation of the Ras/mitogen-activated protein kinase signaling pathway promotes androgen hypersensitivity in LNCaP prostate cancer cells. Cancer Res. **63:**1981–1989.
3. **Bernards, R., and R. A. Weinberg.** 2002. A progression puzzle. Nature **418:**823.
4. **Cantor, S. B., T. Urano, and L. A. Feig.** 1995. Identification and characterization of Ral-binding protein 1, a potential downstream target of Ral GTPases. Mol. Cell. Biol. **15:**4578–4584.
5. **Chambers, A. F., A. C. Groom, and I. C. MacDonald.** 2002. Dissemination and growth of cancer cells in metastatic sites. Nat. Rev. Cancer **2:**563–572.
6. **Chien, Y., and M. A. White.** 2003. RAL GTPases are linchpin modulators of human tumour-cell proliferation and survival. EMBO Rep. **4:**800–806.
7. **Connolly, J. M., and D. P. Rose.** 1998. Angiogenesis in two human prostate cancer cell lines with differing metastatic potential when growing as solid tumors in nude mice. J. Urol. **160:**932–936.
8. **Feig, L. A.** 2003. Ral-GTPases: approaching their 15 minutes of fame. Trends Cell Biol. **13:**419–425.
9. **Feldman, B. J., and D. Feldman.** 2001. The development of androgen-independent prostate cancer. Nat. Rev. Cancer **1:**34–45.
10. **Fidler, I. J.** 2003. The pathogenesis of cancer metastasis: the 'seed and soil' hypothesis revisited. Nat. Rev. Cancer **3:**453–458.
11. **Fidler, I. J., and M. L. Kripke.** 2003. Genomic analysis of primary tumors does not address the prevalence of metastatic cells in the population. Nat. Genet. **34:**23–25.
12. **Frankel, P., A. Aronheim, E. Kavanagh, M. S. Balda, K. Matter, T. D. Bunney, and C. J. Marshall.** 2005. RalA interacts with ZONAB in a cell density-dependent manner and regulates its transcriptional activity. EMBO J. **24:**54–62.
13. **Gonzalez-Garcia, A., C. A. Pritchard, H. F. Paterson, G. Mavria, G. Stamp, and C. J. Marshall.** 2005. RalGDS is required for tumor formation in a model of skin carcinogenesis. Cancer Cell **7:**219–226.
14. **Guise, T. A.** 1997. Parathyroid hormone-related protein and bone metastases. Cancer **80:**1572–1580.
15. **Ikediobi, O. N., H. Davies, G. Bignell, S. Edkins, C. Stevens, S. O'Meara, T. Santarius, T. Avis, S. Barthorpe, L. Brackenbury, G. Buck, A. Butler, J. Clements, J. Cole, E. Dicks, S. Forbes, K. Gray, K. Halliday, R. Harrison, K. Hills, J. Hinton, C. Hunter, A. Jenkinson, D. Jones, V. Kosmidou, R. Lugg, A. Menzies, T. Mironenko, A. Parker, J. Perry, K. Raine, D. Richardson, R. Shepherd, A. Small, R. Smith, H. Solomon, P. Stephens, J. Teague, C. Tofts, J. Varian, T. Webb, S. West, S. Widaa, A. Yates, W. Reinhold, J. N. Weinstein, M. R. Stratton, P. A. Futreal, and R. Wooster.** 2006. Mutation analysis of 24 known cancer genes in the NCI-60 cell line set. Mol. Cancer Ther. **5:**2606–2612.
16. **Kang, Y., P. M. Siegel, W. Shu, M. Drobnjak, S. M. Kakonen, C. Cordon-Cardo, T. A. Guise, and J. Massague.** 2003. A multigenic program mediating breast cancer metastasis to bone. Cancer Cell **3:**537–549.
17. **Lim, K. H., A. T. Baines, J. J. Fiordalisi, M. Shipitsin, L. A. Feig, A. D. Cox, C. J. Der, and C. M. Counter.** 2005. Activation of RalA is critical for Ras-induced tumorigenesis of human cells. Cancer Cell **7:**533–545.
18. **Lim, K. H., K. O'Hayer, S. J. Adam, S. D. Kendall, P. M. Campbell, C. J. Der, and C. M. Counter.** 2006. Divergent roles for RalA and RalB in malignant growth of human pancreatic carcinoma cells. Curr. Biol. **16:**2385–2394.
19. **Logothetis, C. J., and S. H. Lin.** 2005. Osteoblasts in prostate cancer metastasis to bone. Nat. Rev. Cancer **5:**21–28.
20. **Minn, A. J., G. P. Gupta, P. M. Siegel, P. D. Bos, W. Shu, D. D. Giri, A. Viale, A. B. Olshen, W. L. Gerald, and J. Massague.** 2005. Genes that mediate breast cancer metastasis to lung. Nature **436:**518–524.
21. **Minn, A. J., Y. Kang, I. Serganova, G. P. Gupta, D. D. Giri, M. Doubrovin, V. Ponomarev, W. L. Gerald, R. Blasberg, and J. Massague.** 2005. Distinct organ-specific metastatic potential of individual breast cancer cells and primary tumors. J. Clin. Investig. **115:**44–55.
22. **Miric, A., M. Banks, D. Allen, J. Feighan, C. A. Petersilge, J. R. Carter, and J. T. Makley.** 1998. Cortical metastatic lesions of the appendicular skeleton from tumors of known primary origin. J. Surg. Oncol. **67:**255–260.
23. **Moskalenko, S., D. O. Henry, C. Rosse, G. Mirey, J. H. Camonis, and M. A. White.** 2002. The exocyst is a Ral effector complex. Nat. Cell Biol. **4:**66–72.
24. **Mundy, G. R.** 2002. Metastasis to bone: causes, consequences and therapeutic opportunities. Nat. Rev. Cancer **2:**584–593.
25. **Nelson, W. G., A. M. De Marzo, and W. B. Isaacs.** 2003. Prostate cancer. N. Engl. J. Med. **349:**366–381.
26. **Nemeth, J. A., J. F. Harb, U. Barroso, Jr., Z. He, D. J. Grignon, and M. L. Cher.** 1999. Severe combined immunodeficient-hu model of human prostate cancer metastasis to human bone. Cancer Res. **59:**1987–1993.
27. **Ohta, Y., N. Suzuki, S. Nakamura, J. H. Hartwig, and T. P. Stossel.** 1999. The small GTPase RalA targets filamin to induce filopodia. Proc. Natl. Acad. Sci. USA **96:**2122–2128.
28. **Orr, F. W., and H. H. Wang.** 2001. Tumor cell interactions with the microvasculature: a rate-limiting step in metastasis. Surg. Oncol. Clin. N Am. **10:**357–381.
29. **Oxford, G., C. R. Owens, B. J. Titus, T. L. Foreman, M. C. Herlevsen, S. C. Smith, and D. Theodorescu.** 2005. RalA and RalB: antagonistic relatives in cancer cell migration. Cancer Res. **65:**7111–7120.
30. **Ponomarev, V., M. Doubrovin, I. Serganova, J. Vider, A. Shavrin, T. Beresten, A. Ivanova, L. Ageyeva, V. Tourkova, J. Balatoni, W. Bornmann, R. Blasberg, and J. Gelovani Tjuvajev.** 2004. A novel triple-modality reporter gene for whole-body fluorescent, bioluminescent, and nuclear noninvasive imaging. Eur. J. Nucleic Med. Mol. Imaging **31:**740–751.
31. **Ramaswamy, S., K. N. Ross, E. S. Lander, and T. R. Golub.** 2003. A molecular signature of metastasis in primary solid tumors. Nat. Genet. **33:**49–54.
32. **Repasky, G. A., E. J. Chenette, and C. J. Der.** 2004. Renewing the conspiracy theory debate: does Raf function alone to mediate Ras oncogenesis? Trends Cell Biol. **14:**639–647.
33. **Rodriguez-Viciana, P., P. H. Warne, A. Khwaja, B. M. Marte, D. Pappin, P. Das, M. D. Waterfield, A. Ridley, and J. Downward.** 1997. Role of phospho-

inositide 3-OH kinase in cell transformation and control of the actin cytoskeleton by Ras. Cell **89:**457–467.
34. **Ruoslahti, E.** 2004. Vascular zip codes in angiogenesis and metastasis. Biochem. Soc. Trans. **32:**397–402.
35. **Russell, P. J., S. Bennett, and P. Stricker.** 1998. Growth factor involvement in progression of prostate cancer. Clin. Chem. **44:**705–723.
36. **Shipitsin, M., and L. A. Feig.** 2004. RalA but not RalB enhances polarized delivery of membrane proteins to the basolateral surface of epithelial cells. Mol. Cell. Biol. **24:**5746–5756.
37. **Stone, K. R., D. D. Mickey, H. Wunderli, G. H. Mickey, and D. F. Paulson.** 1978. Isolation of a human prostate carcinoma cell line (DU 145). Int. J. Cancer **21:**274–281.
38. **van 't Veer, L. J., H. Dai, M. J. van de Vijver, Y. D. He, A. A. Hart, M. Mao, H. L. Peterse, K. van der Kooy, M. J. Marton, A. T. Witteveen, G. J. Schreiber, R. M. Kerkhoven, C. Roberts, P. S. Linsley, R. Bernards, and S. H. Friend.** 2002. Gene expression profiling predicts clinical outcome of breast cancer. Nature **415:**530–536.
39. **Ward, Y., W. Wang, E. Woodhouse, I. Linnoila, L. Liotta, and K. Kelly.** 2001. Signal pathways which promote invasion and metastasis: critical and distinct contributions of extracellular signal-regulated kinase and Ral-specific guanine exchange factor pathways. Mol. Cell. Biol. **21:**5958–5969.
40. **Weber, M. J., and D. Gioeli.** 2004. Ras signaling in prostate cancer progression. J. Cell Biochem. **91:**13–25.
41. **Weiss, L.** 1992. Comments on hematogenous metastatic patterns in humans as revealed by autopsy. Clin. Exp. Metastasis **10:**191–199.
42. **Weiss, L., K. Haydock, J. W. Pickren, and W. W. Lane.** 1980. Organ vascularity and metastatic frequency. Am. J. Pathol. **101:**101–114.
43. **White, M. A., C. Nicolette, A. Minden, A. Polverino, L. Van Aelst, M. Karin, and M. H. Wigler.** 1995. Multiple Ras functions can contribute to mammalian cell transformation. Cell **80:**533–541.